Structure of colloidal gels at intermediate concentrations: the role of competing interactions

Structure of colloidal gels at intermediate concentrations: the role of competing interactions

Ronja F. Capellmann[a], Néstor E. Valadez-Pérez[b], Benedikt Simon[a], Stefan U. Egelhaaf[a], Marco Laurati[a,b] and Ramón Castañeda-Priego[b]

Received Xth XXXXXXXXXX 20XX, Accepted Xth XXXXXXXXX 20XX
First published on the web Xth XXXXXXXXXX 200X
DOI: 10.1039/b000000x

Colloidal gels formed by colloid-polymer mixtures with intermediate volume fraction ($\phi_c \approx 0.4$) are investigated by confocal microscopy. In addition, we have performed Monte Carlo simulations based on a simple effective pair potential that includes a short-range attractive contribution representing depletion interactions, and a longer-ranged repulsive contribution describing the electrostatic interactions due to the presence of residual charges. Despite neglecting non-equilibrium effects, experiments and simulations yield similar gel structures, characterised by, e.g., the pair, angular and bond distribution functions. We find that the structure hardly depends on the strength of the attraction if the electrostatic contribution is fixed, but changes significantly if the electrostatic screening is changed. This delicate balance between attractions and repulsions, which we quantify by the second virial coefficient, also determines the location of the gelation boundary.

1 Introduction

Competing short-range attractive and long-range repulsive interactions between macromolecules are encountered in a vast number of systems in biology, medicine and materials science, namely, protein solutions[1–3], therapeutic monoclonal antibodies[4–7], colloidal gels[8,9] and nanoparticle suspensions[10], among others.

Mixtures of spherical colloids and non-adsorbing polymers dispersed in a solvent are often used as experimental models to investigate the behaviour of more complex systems with competing interactions. This is due to the fact that each contribution of the interaction potential can be tuned through the polymer concentration and size[11], as well as the particle charge and salt concentration[12], i.e., the degree of electrostatic screening. The short-range attractions arise due to entropy effects mediated by a second component[13,14], i.e., the polymers, whereas long-range repulsions are caused by residual charges on the particle surface. In the presence of short-range attractions, fluid phases, fluid-crystal coexistence and crystalline phases can be observed in equilibrium[15,16], while gels and glassy structures are found under non-equilibrium conditions[8,11,16,17]. In contrast, by reducing the degree of screening, additional states are observed, like fluids of clusters, gels and Wigner glasses[18,19].

Gels are amorphous solids in which mechanical stability is achieved through the self-assembly of a load-bearing network structure. Since gels are non-equilibrium states, their properties depend on the preparation history. Different paths to the non-equilibrium gel states have been discussed. In the limit of purely attractive interactions, for example, arrested phase separation[20], glass-like arrest[21,22], rigidity percolation[23] and the formation of locally favoured structures[24] have been proposed. In the presence of electrostatic interactions, cluster aggregation into a percolating network[19,25–27] has been suggested, with recent results indicating the importance of directed rather than continuous percolation[28].

A common feature of the gel state is structural heterogeneity with a characteristic length scale, which depends on the colloid volume fraction ϕ_c, the parameters controlling the interaction potential and, due to non-equilibrium conditions, the preparation procedure. Structures of cluster fluids and colloidal gels have been reported over a broad range of ϕ_c and potential parameters, both in the moderately screened[19,25–27,29–31] and strongly screened[8,20,22,32–34] cases. For small ϕ_c, the structures observed in confocal microscopy experiments[20,28,35,36] were satisfactorily modelled using either an Asakura-Oosawa (AO) potential[13,14] in the strongly screened case[20] or a combination of the AO and Yukawa potentials in the moderately screened case[28,35,36]. Nevertheless, recent experimental results show that effects of anisotropic charge screening might lead to deviations from the behaviour predicted on the basis of this combination of potentials[37].

[a] *Condensed Matter Physics Laboratory, Heinrich Heine University, Universitätsstr. 1, 40225 Düsseldorf, Germany*
[b] *División de Ciencias e Ingenierías, Campus León, Universidad de Guanajuato, Loma del Bosque 103, Lomas del Campestre, 37150 León, Guanajuato, Mexico; E-mail: mlaurati@fisica.ugto.mx, ramoncp@fisica.ugto.mx*

However, at intermediate and large $\phi_c > 0.2$, a direct comparison between simulations or theory and experiments has only been reported by Shah and coworkers[38], where no satisfactory agreement between PRISM theory calculations and experimental structure factors could be obtained in the gel state. Hence, gelation in colloids with competing interactions has been studied extensively in the last few years[28,35,36], but at intermediate and large concentrations several aspects can complicate a description of the structural properties of gel states in terms of the underlying interparticle potential that still are not fully understood. For instance, the possible importance of three-body interactions, the effects of crowding, as well as concentration effects on the polymer size have to be taken into account. Furthermore, the influence of the route leading to the final (non-equilibrium) gel structure might be important and hence, at the same sample composition, different gel structures might occur. In addition, typical experimental colloidal systems are polydisperse. Under these non-equilibrium conditions, only a description based on an *effective* interparticle interaction potential is possible and, furthermore, the potential is hard to accurately determine[39] through, for example, reverse Monte Carlo and integral equation techniques. In particular, these techniques have not been established yet for concentrated polydisperse colloidal systems.

In this contribution, we address the relation between the effective interparticle interactions and the structure of the gel. As far as we are aware, here we provide for the first time a quantitative description of the effective interaction between particles that determines the local properties of the dispersion under non-equilibrium conditions. In particular, a combination of a short-range attraction and longer-ranged repulsion has been used to describe the effective interaction potential in intermediate volume fraction colloidal fluids and gels with $\phi_c \sim 0.40$. The parameters of the potential have been obtained by fitting only the simulated radial distribution function, $g(r)$, to the measured $g(r)$. Based on the determined potential, we have calculated further quantities describing the structure, such as the angular distribution function $P(\theta)$ and the nearest-neighbour distribution function $P(n_b)$, as well as the state diagram. As mentioned above, despite of the difficulties to determine an effective interaction potential under non-equilibrium conditions, the structures of the colloidal fluids and gels appear accurately described based on the competing short-range attractive and longer-ranged repulsive interaction potential. We furthermore demonstrate that the short-range depletion attraction induced by the polymers can be reproduced by a short-range square-well potential, following the extended law of corresponding states[40]. Moreover, it is crucial to consider the electrostatic repulsion to properly reproduce the structure and morphology of the gel structure although the investigated experimental systems were located in the regime between moderate and strong screening. The delicate balance between the attractive and repulsive contributions in the effective pair potential has a significant effect on the location of the gelation boundary.

2 Materials and Methods

2.1 Experimental details

We have investigated mixtures of polymethylmethacrylate (PMMA) hard-sphere like particles fluorescently labelled with 7-nitrobenzo-2-oxa-1,3-diazole-methylmethacrylate (NBD-MMA) and linear polystyrene (PS, from Polymer Laboratories). The average diameter of the PMMA particles, $\sigma = 1720$ nm, and their polydispersity of about 7% were determined by static and dynamic light scattering using very dilute samples. The radius of gyration of the PS (molecular weight $M_w = 3 \times 10^6$ g/mol with $M_w/M_n = 1.17$) in the solvent mixture used was estimated to be $r_g = 65.4$ nm[41]. In a dilute solution, this implies a polymer-colloid size ratio $\xi = 2\,r_g/\sigma = 0.076$. The effective polymer-colloid size ratio ξ^* (Table 1) was calculated according to the Generalised Free Volume Theory (GFVT)[42,43], taking into account the concentration dependence of the radius of gyration and mesh size of the polymer in the semidilute regime.

The particles and polymers were dispersed in a solvent mixture of cis-decalin and cycloheptylbromide, which closely matched the refractive index and the density of the colloidal particles. The density difference $\Delta\rho = \rho_c - \rho_s$ between the colloidal particles and the solvent mixture was estimated to be $\Delta\rho/\rho_c \lesssim 10^{-3}$, as no sedimentation was observed after centrifuging the sample for 24 h with 3500 rpm corresponding to an acceleration of about $1800\,g$ with g the acceleration due to gravity. From this density difference, the gravitational Peclet number $Pe \equiv v_s\,\sigma/(2\,D)$, with the sedimentation velocity v_s and the free diffusion coefficient D, was estimated to be $Pe \lesssim 7 \times 10^{-3}$ at 23 °C. In this solvent mixture, colloidal particles acquire a small charge, which is partially screened by the addition of tetrabutylammoniumchloride (TBAC)[12,44]. TBAC was added to the solvent mixture before preparing colloid and polymer stock solutions. Then, the solvent mixture was put on a flask shaker for at least 3 days to dissolve the salt.

The colloid stock solution was prepared by diluting a spun-down sediment, for which we initially assumed a volume fraction $\phi_c = 0.64$. Subsequently, the actual volume fraction of the samples was determined by confocal microscopy using the Voronoi construction to estimate the average volume fraction ϕ_c. Polymer stock solutions were prepared by adding the solvent mixture to dry polymer and the polymer concentration c_p (mass/volume) of the solution was calculated from the weighed masses of the solvent and polymer, and their corre-

Sample	ϕ_c^{exp}	$c_s\,[mM]$	$c_p\,[c^*]$	$c_p^{free}\,[c^*]$	ξ^*
Set A					
1	0.39	4.9	0.0	0.0	–
2	0.41	4.5	0.8	1.51	0.04
3	0.39	4.5	1.0	1.75	0.03
4	0.39	4.5	1.1	1.81	0.03
5	0.40	4.5	2.0	3.37	0.02
Set B					
6	0.44	4.8	0.0	0.0	–
7	0.40	4.8	0.0	0.0	–
8	0.43	5.3	0.1	0.23	0.08
9	0.38	5.3	0.1	0.23	0.08
10	0.43	5.2	1.4	2.84	0.03
11	0.44	5.3	1.4	3.25	0.02
12	0.42	5.2	1.7	3.38	0.02

Table 1 Colloid-polymer samples analysed in this work. ϕ_c^{exp} is the colloid volume fraction determined from the particle coordinates (via confocal microscopy) using the average diameter, c_s and c_p the concentrations of salt and polymer, respectively, c_p^{free} the polymer concentration in the volume not occupied by the colloids and ξ^* the resulting effective polymer-colloid size ratio, both estimated by Generalised Free Volume Theory[42,43]. Note that the two sets were prepared independently and might thus reflect different preparation paths.

sponding densities. The polymer overlap concentration c_p^* has been estimated by $c_p^* = 3M_w/4\pi N_A r_g^3$ with Avogadro's number N_A. Colloid-polymer mixtures were prepared by mixing appropriate amounts of colloid and polymer stock solutions. Subsequently, samples were vigorously mixed using a vortex shaker and then homogenised in a flask shaker. The compositions of the samples are reported in Table 1. Note that the two sets A and B are prepared independently and hence the composition and age of the solvent mixtures and in particular the particle charges and effective dissolved salt (TBAC) concentrations might actually be different as well as the details of the preparation path.

Microscopy measurements were performed within an hour after mixing to avoid effects due to ageing. Samples of set A were observed using a VT-Eye confocal unit (Visitech International) mounted on a Nikon Ti-U inverted microscope with a Nikon Plan Apo VC 100× (NA=1.40) oil immersion objective. Samples of set B were imaged with a Nikon A1R-MP confocal unit on an inverted Nikon Ti-E microscope with a Nikon Plan Apo VC 60× (NA=1.40) oil immersion objective. Between 25 and 30 stacks of 151 slices of 512×512 pixels each were recorded in z-steps of 200 nm corresponding to $54 \times 54 \times 30\ \mu m^3$ in the bulk of the sample. The stacks were acquired in less than 20 s per stack. Typically, the observation volume contained about $14,000$ particles. Particle coordinates were obtained from images using standard routines[45], including an algorithm to refine the particle coordinates[46]. Only particles whose centres were at least 4σ from the edges of the observation volume were considered in order to avoid boundary effects.

2.2 Effective interaction potentials and computer simulations

Attractive depletion interactions induced by non-adsorbing polymers were modelled using a short-range square-well (SW) potential[47,48]. This is simpler than the well-known Asakura-Oosawa (AO) potential[13,14]. Based on the extended law of corresponding states proposed by Noro and Frenkel[40], we have shown that the phase diagrams obtained with the AO and SW potentials are similar[48] and can also be used to describe the phase behaviour of more complex systems, such as proteins[49,50]. The SW potential has the following form[47,48],

$$u_{ij}^{SW}(r) = \begin{cases} \infty & r < \sigma_{ij} \\ -\epsilon & \sigma_{ij} \le r \le \lambda\sigma_{ij} \\ 0 & r > \lambda\sigma_{ij}, \end{cases} \quad (1)$$

where r is the centre-centre distance between colloids of diameters σ_i and σ_j, with $\sigma_{ij} = (\sigma_i + \sigma_j)/2$, ϵ is the well depth given in units of the thermal energy $k_B T$ and λ characterises the attraction range. The latter can be related to the effective polymer-colloid size ratio ξ^* of the experimental system, $\lambda \approx \sigma_{ij}/\sigma + \xi^*$ (Table 1).

The colloidal particles carried a net charge, which was screened by adding salt[51–53]. When the degrees of freedom of the small counterions are integrated out, the pure Coulombic interaction between colloids is replaced by a renormalised interaction potential of the Yukawa form[51–53],

$$u_{ij}^{sC}(r) = Z_{ij}^2 \frac{\exp\left[-\kappa(r - \sigma_{ij})\right]}{r/\sigma_{ij}}, \quad (2)$$

where κ is the inverse of the Debye length[51–53] and Z_{ij}^2 is the strength of the repulsion between the particles i and j in units of $k_B T$,

$$Z_{ij}^2 = \frac{Q_i^{eff} Q_j^{eff}}{(1 + \kappa\sigma_{ij}/2)^2} \frac{\lambda_B}{\sigma_{ij}}, \quad (3)$$

with $Q_{i,j}^{eff}$ the net charge of species i or j in units of the electron charge and λ_B the Bjerrum length[51–53]. The definitions of the pair potentials, Eqs. (1) and (2), allowed us to include the size polydispersity[54].

The total interaction between pairs of particles is described by a combination (not the sum) of the contributions in Eqs. (1) and (2). For separations larger than $\lambda\sigma_{ij}$, the interaction is purely repulsive and is given by Eq. (2). At short distances, lower than $\lambda\sigma_{ij}$, we assume that the interaction is dominated

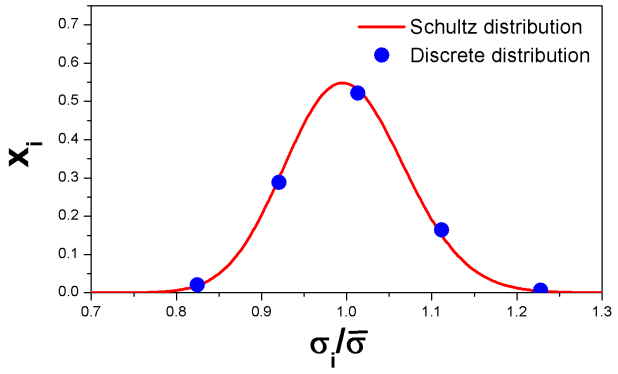

Fig. 1 Number fraction x_i of particles with diameter σ_i following a Schulz distribution (solid line) and discrete distribution with five populations used in the Monte Carlo simulations (symbols), respectively.

by the attractive depletion interaction, which we model with a SW, Eq. (1). Our choice of this simple effective model potential does not represent the true potential of the physical systems we are investigating. However, as will be shown, it is able to reproduce the experimental structures and allows us to separately study the contribution of the repulsion and of the attraction.

We have performed Monte Carlo (MC) computer simulations in the canonical ensemble (NVT) for systems with $N = 2916$ particles having 7% of polydispersity. The latter was taken into account by considering five populations of particles whose size and number fraction follow a discrete Schulz distribution[54,55], see Fig. 1. The number fraction, $x_i = N_i/N$, is the relative population of particles with diameter σ_i; N_i and N are the number of particles of species i and the total number of particles in the system, respectively. The standard Metropolis algorithm was used to generate and accept new particle configurations[56,57]. We ran MC simulations for 5×10^8 MC steps to reach a steady-state and additional 5×10^8 MC steps to measure the structure. In both stages, new configurations were accepted with a probability of 30%. In all simulations, thermal equilibrium was reached after a few millions of MC steps.

3 Results

3.1 Structure of the fluids without polymer

The spatial arrangement of particles around a central one is characterised by the radial distribution function, $g(r)$. Fig. 2a shows the experimental $g(r)$ determined for samples without polymer (samples 1, 6 and 7, see Table 1). In all cases, it shows the structural characteristics of a fluid, i.e., a first peak roughly corresponding to the average particle distance $(\pi/6\phi_c)^{1/3}\sigma \approx 1.08\sigma$, and successive peaks that correspond to further shells of neighbours, until correlation is lost at larger distances where $g(r)$ tends to 1.

The experimental $g(r)$ is compared to MC simulations for hard-spheres with a polydispersity of about 7%. Simulating hard-sphere systems at high concentrations is difficult because non-overlapping initial configurations need to be generated. In a monodisperse system, one can initiate simulations with particles in a crystalline array, which melts during the simulation with no overlaps occurring between particles. In a polydisperse system, however, some big particles might be difficult to place in a non-overlaping configuration. To overcome this technical problem, the hard-sphere potential has been replaced by the potential $u_{ij}^{\mathrm{HS}}(r) = \left(r/\sigma_{ij}\right)^{-10000}$, where the large exponent results in a hard-sphere-like interaction. Fig. 2a shows that the agreement between simulations and experiments is not satisfactory, especially at short separations, $r \approx \sigma$. The average distance, described by the position of the first peak in $g(r)$, is about σ in the simulations, while it is slightly larger in the experiments. This indicates that the effective size of the particles is larger than σ. This can result from residual charges. Therefore, we have also performed MC simulations including a repulsive Yukawa potential, see Eq. (2). The parameters of the Yukawa potential were estimated using the Poisson-Boltzmann equation and assuming that all particles have the same diameter[51]. This led to a prefactor $Z_{ij}^2 = 6.0$ and screening parameter $\kappa\sigma = 15$ and 30, corresponding to an effective charge $Q^{\mathrm{eff}} \approx 273$ and 514, for sets A and B, respectively, see Table 2. This effective charge is consistent with previous measurements[36]. The screening $\kappa\sigma$ differs by a factor of 2, although the salt concentration c_{s} in both sets is similar. This might be related to the fact that the dissolution of salt in the solvent mixture is limited and slow, and therefore a different amount of salt might actually be dissolved in the two sets, despite of the added salt concentrations c_{s} being comparable. Furthermore, differences in the dissolution process imply different preparation paths which might affect the observed gel structure. Nevertheless, the excellent agreement between experiments and simulations (Fig. 2b) indicates that the amount of particle charge has an important effect on the structure of the dispersion due to the long range of the electrostatic interactions in organic solvents having small relative permittivities.

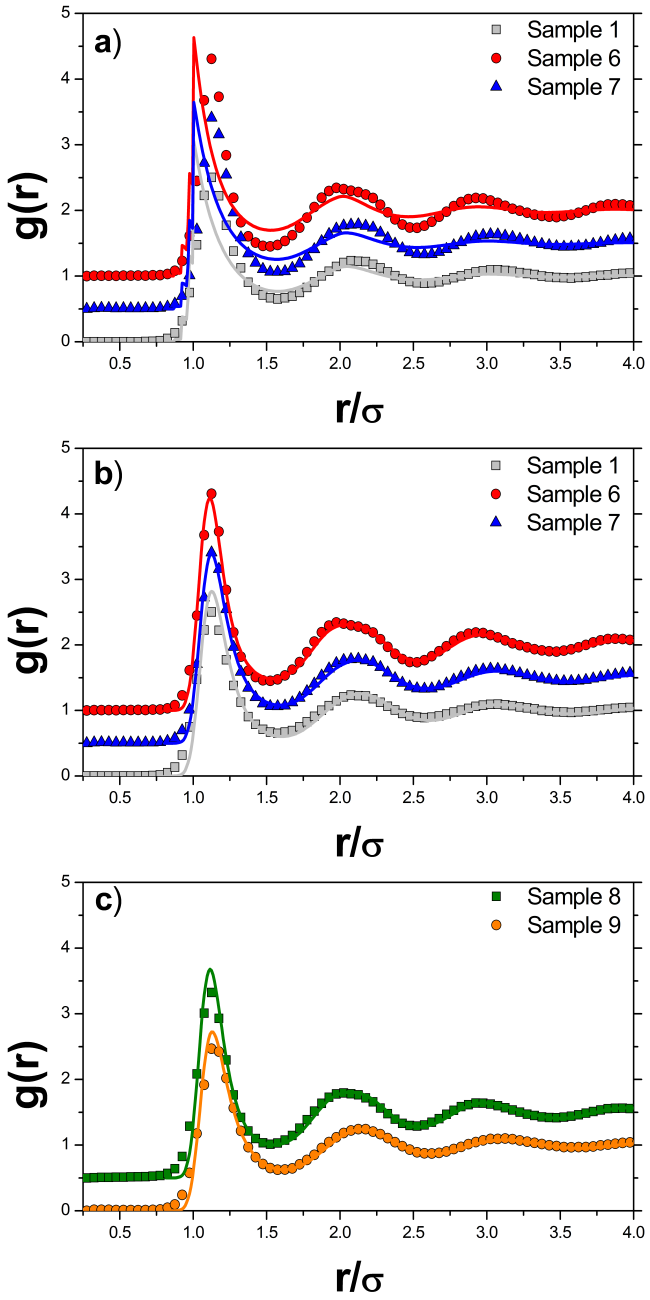

Fig. 2 a) Radial distribution function $g(r)$ for a) polymer-free samples 1, 6 and 7 (symbols, Table 1) and MC simulation results for polydisperse hard-spheres (solid lines). b) Same as in a) but with simulation results for charged polydisperse particles interacting through a Yukawa pair potential (Eq. (2)). c) Samples 8 and 9 with low polymer concentration (symbols, Table 1) and simulation results for particles interacting through a SW (Eq. (1)) and Yukawa pair potential (Eq. (2)) (solid lines). Curves are vertically shifted for clarity.

The electrostatic interaction also affects the subsequent peaks, which are now well-reproduced. This indicates the need to include the electrostatic contribution (Eq. (2)) together with the hard-sphere interaction to correctly represent the repulsive interactions between colloids.

We assume that the parameters of the Yukawa potential remain constant upon addition of polymer, although at larger polymer concentrations the high packing of particles in the gels might modify the charge distribution. However, the very good agreement obtained between experiments and simulations shown below supports the validity of this assumption.

3.2 Structure of the fluid at low polymer concentrations

The structure of samples containing a small amount of polymer, $c_\mathrm{p}/c_\mathrm{p}^* = 0.1$ (samples 8 and 9, Fig. 2c), was also experimentally determined. Due to the presence of polymer, attractive interactions are present and result in a non-zero, although very small, ϵ. Nevertheless, $g(r)$ is very similar to that of the purely repulsive systems without polymer. This suggests that repulsive interactions dominate at low polymer concentrations. In fact, $g(r)$ can be well reproduced in simulations using only the repulsive Yukawa potential with the same parameters as for the case without polymer (except $\epsilon = 0$; data not shown).

3.3 Structure of the gel at high polymer concentrations

3.3.1 Radial distribution function $g(r)$. Fig. 3 shows $g(r)$ for samples with high polymer concentrations $c_\mathrm{p}/c_\mathrm{p}^* \geq 0.8$. The presence of significant attractions completely changes the shape of $g(r)$ compared to the samples without and with only a small amount of polymer (Fig. 2). The first peak becomes sharper. The position of the first minimum of $g(r)$, which appears at $r/\sigma \approx 1.1$, can be linked to the effective range of the attraction, characterised by $\lambda - 1$; the minimum is less pronounced for set B than for set A. The broad second peak is a typical feature of gels and is related to the broad distribution of distances to particles in the second shell caused by the heterogenous structure of the local clusters[29,32]. Beyond the second maximum, i.e. for distances beyond about 2.5σ, $g(r)$ quickly approach unity, whereas the oscillations extend to much larger r for the samples without or with less polymer.

In MC simulations, the effective interparticle interactions were modelled through the attractive SW potential, Eq. (1), and repulsive Yukawa potential, Eq. (2). The values of the parameters characterising the Yukawa contribution are taken from the samples without polymer ($\kappa\sigma = 15$ and 30, $Q^\mathrm{eff} \approx 273$ and 514 for sets A and B, respectively, see Table 2). For the range of the attractions, average values $\xi^* \leq \xi' \leq \xi$ are taken resulting in a constant $\lambda = \sigma_{ij}/\sigma + \xi'$ for each set (Table

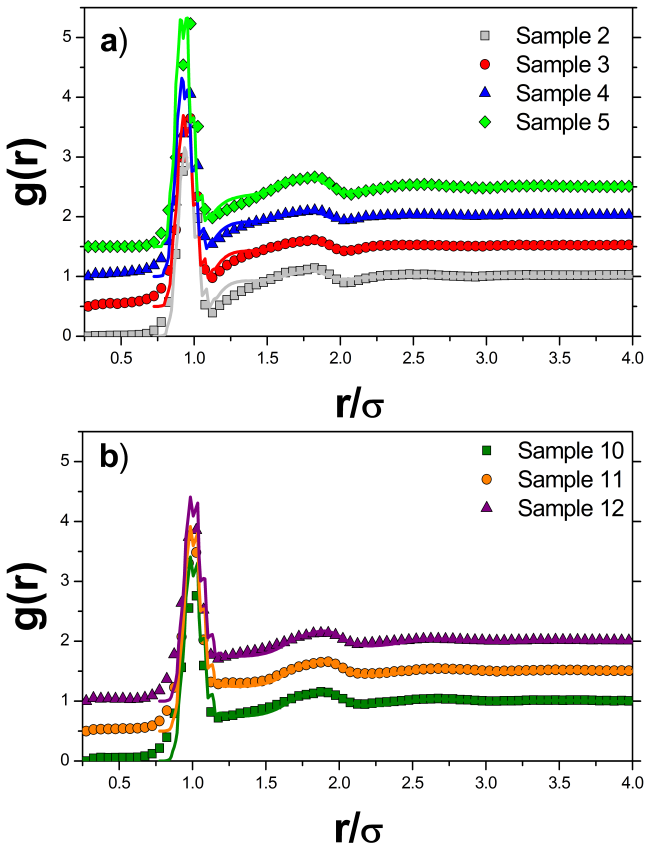

Fig. 3 Radial distribution function $g(r)$ for samples with high polymer concentrations (as indicated, Table 1), obtained in experiments (symbols) and MC simulations (solid lines). Curves are vertically shifted for clarity.

Sample	σ_c/σ	ϵ	λ	Q^{eff}	$\kappa\sigma$	B_2^*
Set A						
1*	1.0	0.0	–	514	30	1.25
2	0.93	0.83	1.03	273	15	0.64
3	0.93	0.83	1.03	273	15	0.64
4	0.93	0.91	1.03	273	15	0.58
5	0.93	1.11	1.03	273	15	0.40
Set B						
6*	1.0	0.0	–	514	30	1.25
7*	1.0	0.0	–	514	30	1.25
8*	1.0	0.0	–	514	30	1.25
9*	1.0	0.0	–	514	30	1.25
10	0.97	1.33	1.07	514	30	-0.31
11	0.97	1.33	1.07	514	30	-0.31
12	0.97	1.43	1.07	514	30	-0.44

Table 2 Values used in the MC simulations to describe the experimentally determined $g(r)$ for the samples given in Table 1. Average effective hard-sphere diameter σ_c, attraction strength ϵ, attraction range λ, effective charge Q^{eff} and inverse screening length κ. The $(*)$ indicates that the interaction between particles was modelled by a pure repulsive potential, resulting in B_2^* values larger than 1.

2). Several simulations have been performed with different values of the depth of the square well ϵ to find the best fit to the experimental $g(r)$. Samples with high polymer concentrations cannot be accurately simulated using an average diameter σ = 1720 nm but, to match the experimental $g(r)$, a slightly smaller effective diameter σ_c was considered, which is within the uncertainties of the experimental value and the chosen size distribution. The reduction of the effective diameter in the gels seems to indicate a certain degree of softness of the particles. We have hence considered a soft-core potential represented by $(r/\sigma_c)^{-9}$ to model this degree of softness. The stronger reduction of the diameter in set A than B is associated with less screening of the electrostatic interaction, possibly indicating a relation between the two quantities. The fitted values of σ_c and ϵ are reported in Table 2. With these values, the MC simulations agree well with the experimental results over the whole range of r values. This indicates that the effective potential reproduces the experimental structure at short and long interparticle separations. Table 2 also indicates that the well depth ϵ is a function of polymer, c_{p}, and, to some extent, colloid, ϕ_{c}, concentration.

3.3.2 Effective colloid-colloid interaction potential $u(r)$. The interactions in the colloid-polymer mixtures were approximated by a combination of a SW and Yukawa potential, given by Eqs. (1) and (2), respectively, where the hard-sphere infinite repulsion at contact in the SW potential has been slightly softened due to technical issues as discussed above. The parameters of the potentials have been determined by fitting the corresponding $g(r)$ to the experimental data (Figs. 2, 3 and Table 2). Note that these are effective interaction potentials. They depend on the sample compositions but, due to the non-equilibrium nature of gels, are also affected by the preparation histories. A different sample preparation procedure might lead to a different gel structure, here characterized by $g(r)$, and hence a different effective interaction potential, although the final sample composition might be identical. The dependence on the preparation path is, at least partially, responsible for the different fit parameters of sets A and B, although their compositions are not very different.

The combination of SW and Yukawa potential is compared to the potential of mean force, $w(r) = -k_{\mathrm{B}}T \ln g(r)$ (Fig. 4a). This potential is an accurate representation of the effective potential between pairs of colloidal particles, $u(r)$, in a low concentration system[58]. At higher concentrations, $w(r)$ is a crude approximation of the effective potential $u(r)$ but gives some insights on its features. The main features of $w(r)$ are reproduced by the combination of a SW and Yukawa po-

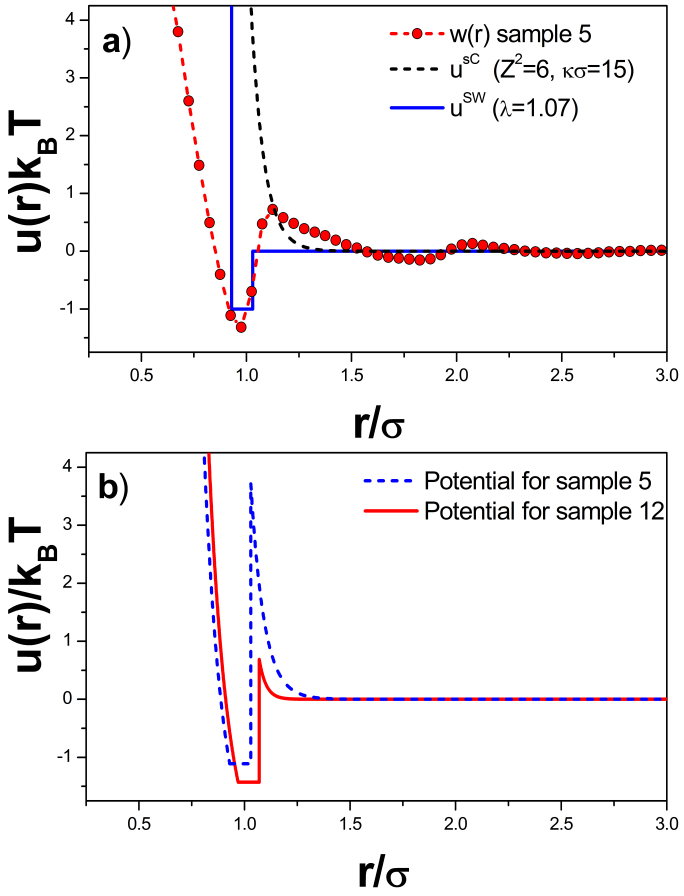

Fig. 4 a) Square well $u^{\mathrm{SW}}(r)$ (solid line), Eq. (1), and Yukawa $u^{\mathrm{sC}}(r)$ (dashed line), Eq. (2), potentials and potential of mean-force $w(r) = -k_{\mathrm{B}}T \ln g(r)$ (dashed-symbol) of sample 5. b) Effective colloid-colloid interaction potentials $u(r)/k_{\mathrm{B}}T$ in samples 5 (solid line) and 12 (dashed line), see Table 1.

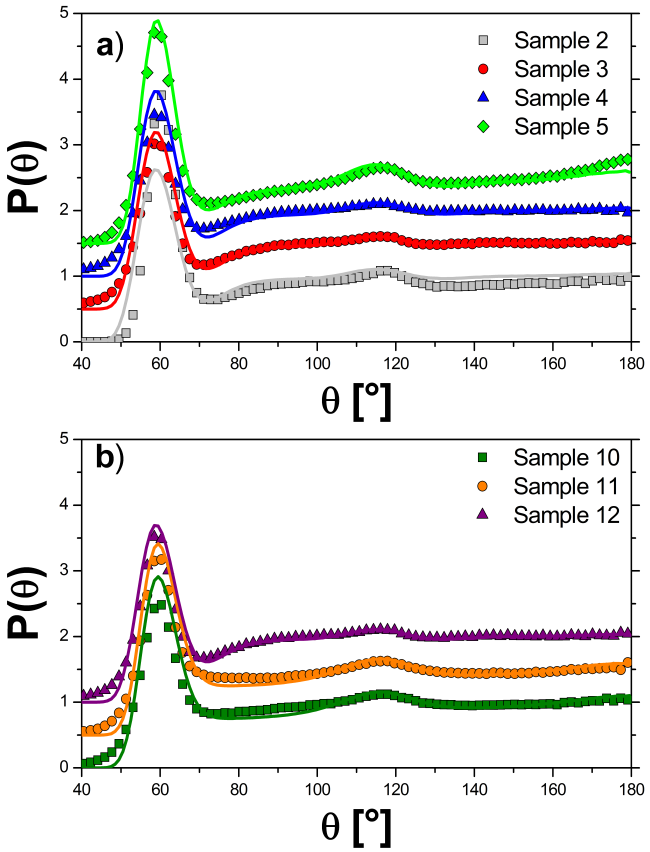

Fig. 5 Angular distribution function $P(\theta)$ for samples with high polymer concentrations (as indicated, Table 1) obtained in experiments (symbols) and MC simulations (solid lines). Curves are vertically shifted for clarity.

tential.

As an example, Fig. 4b displays the optimum effective potentials that describe the local structures of samples 5 (set A) and 12 (set B), respectively. The potential used for sample 5 shows a larger barrier and longer-ranged repulsion compared to sample 12. This illustrates the different amounts of residual charges and screening in the two sets as well as a possible effect of the preparation procedure (Table 2).

3.3.3 Angular distribution function $P(\theta)$. In addition to $g(r)$, it is interesting to determine the angular distribution function $P(\theta)$. This function considers the angle θ between the centre-centre lines of three nearest neighbours. Particles are considered nearest neighbours if their centre-centre distance is smaller than the distance to the first minimum of $g(r)$, which is $r = 1.1\sigma$. The experimentally obtained $P(\theta)$ are shown in Figs. 5 together with the corresponding simulation results. The peak at $\theta \approx 60^{\circ}$ indicates that particles tend to form structures with a triangular geometry. We have shown in previous work that in the presence of short-range attractions and long-range repulsions, these structures are energetically favoured over others[59]. A second smaller peak is located at $\theta \approx 120^{\circ}$, a value that corresponds to a structure where particles lie on two triangles that share an edge.

3.3.4 Nearest-neighbour distribution function $P(n_{\mathrm{b}})$. To gain more insight into the local structural features of the gel and its heterogeneity, we have also determined the nearest-neighbour distribution $P(n_{\mathrm{b}})$; it represents the probability for a particle to have n_{b} neighbours being closer than the cutoff distance $r = 1.1\sigma$. The average value $\langle n_{\mathrm{b}} \rangle$ quantifies how crowded the local environment of a particle is. Previously, it was shown[23] that in a purely attractive system $\langle n_{\mathrm{b}} \rangle = 2.4$ at the gel transition.

The nearest-neighbour distributions $P(n_{\mathrm{b}})$ are shown in Figs. 6a and 6b. One observes that for samples with a high

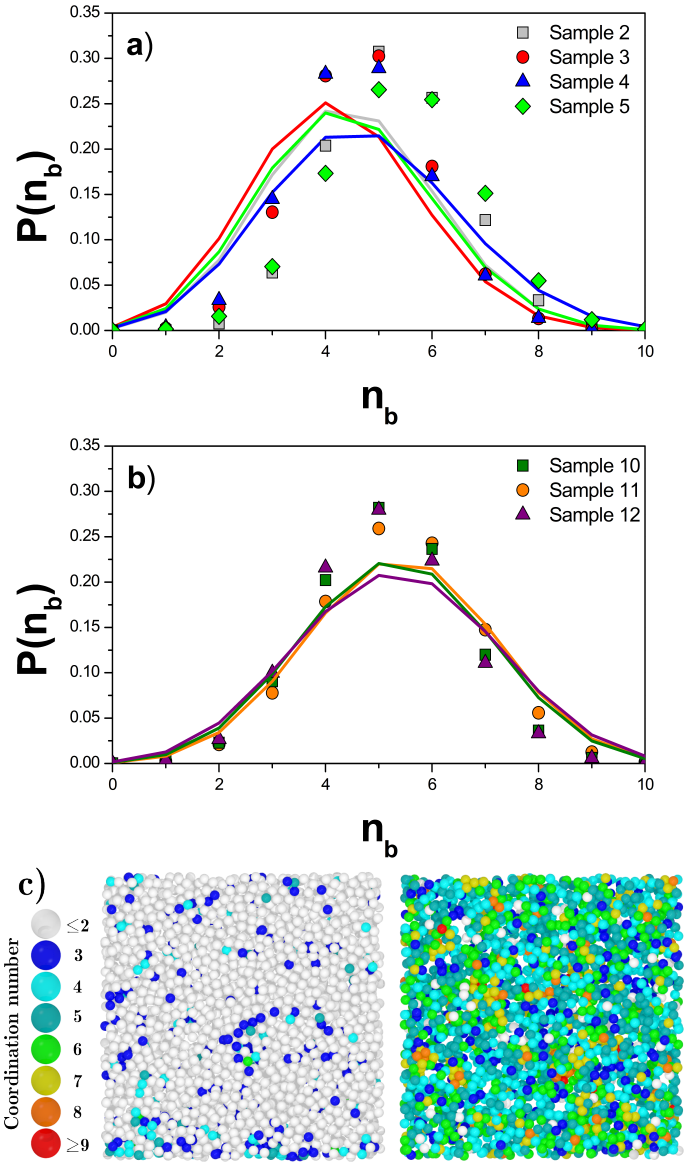

Fig. 6 Distribution of the number of nearest-neighbours, $P(n_\mathrm{b})$, for samples of a) set 1 and b) set 2 as obtained by experiments (symbols) and MC simulations (solid lines). c) Snapshots of slices of samples 1 (left) and 5 (right) as obtained by simulations. The number of neighbours or coordination number is indicated by the colour of the colloids.

polymer concentration, $c_\mathrm{p}/c_\mathrm{p}^* \geq 0.8$, the shape of the distribution is essentially identical and $\langle n_\mathrm{b} \rangle \approx 5$, i.e., larger than the one found in purely attractive (sticky) particles[23]. This indicates local clusters with a highly compact shape. This also implies that the competing interaction potential plays a twofold role: first, the short-range attraction induces particle clustering and, second, the long-range repulsion stabilises the clusters towards network formation, i.e., limits their size, and avoids nucleation and subsequent crystallisation[59]. In contrast, in the presence of only a small amount of polymer, as in samples 8 and 9, the structure is characterised by a small number of neighbours, $\langle n_\mathrm{b} \rangle \approx 2$ (data not shown). It is interesting to note that the neighbour distributions of sets A and B are comparable, despite the structural differences indicated by $g(r)$ and $P(\theta)$. The aforementioned trends can also be seen in snapshots of samples 1 (no polymer) and 5 (highest polymer concentration), displayed in Fig. 6c, with the number of neighbours indicated by the colour. Sample 5 contains a percolated network, i.e., a colloidal gel, whereas there is no network in sample 1. Fig. 6c also illustrates the heterogeneity of the particle distribution in the sample.

The structure of a system can also be visualised by the backbone or network formed by the nearest neighbours. In Fig. 7, slices with thickness 4σ of samples 1, 2 and 5 are considered and nearest neighbours are connected by a line. In sample 1, the connectivity is very low, as expected in the absence of attractions. In samples 2 and 5, particles form triangular structures that are connected into a sample spanning network, as previously reported[25]. Besides, applying the same criterium as the one proposed in Ref.[28], we found evidence that the structures of samples 2 and 5 represent directly percolated networks, as recently proposed for gels with a lower colloid concentration[28] and a smaller $\langle n_\mathrm{b} \rangle$. Samples 9 and 12 show similar results to samples 1 and 5: Sample 9 presents a liquid-like structure, as indicated in Fig. 3, whereas a backbone is present in sample 12, which corresponds to a directed percolated network and presents components that form also triangular structures (data not shown).

3.4 State diagram

Since gels are out of equilibrium states, their structure also depends on the kinetic path followed to reach the gel state. It is therefore interesting to consider how the samples we studied can be located with respect to the equilibrium and the non-equilibrium state diagrams available from literature, and obtained for the specific parameters of our system. Note, however, that care has to be taken when state diagrams based on parameters determined under equilibrium conditions are compared with state diagrams based on parameters of effective interaction potentials determined under non-equilibrium conditions, as in the present case.

We start considering the state diagram of colloid-polymer mixtures with purely attractive interactions[11,16,48]. The topology of the state diagram in the $c_\mathrm{p}/c_\mathrm{p}^*$ *vs* ϕ_c plane depends on the polymer-colloid size ratio ξ; we only consider $\xi \sim 0.1$ (Fig. 8) and $\phi_\mathrm{c} \leq 0.5$, which are the parameters relevant for our study. Previous studies showed that while at small polymer concentrations the system is in a fluid state, with increas-

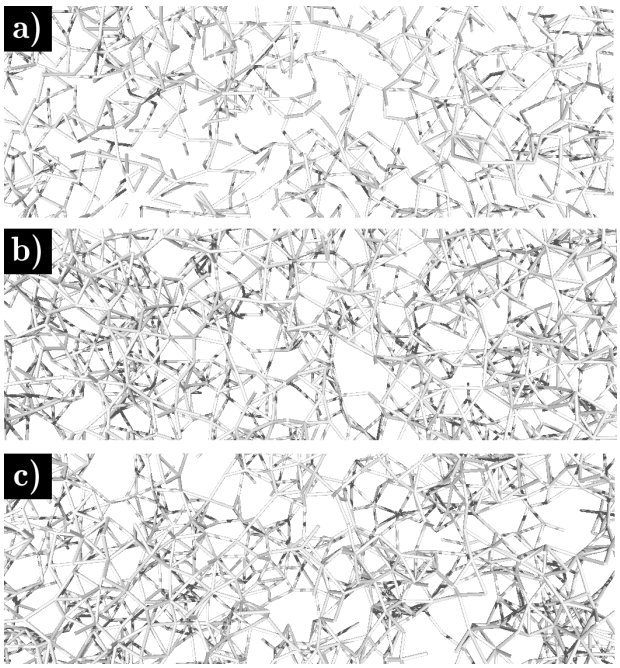

Fig. 7 Network of nearest neighbours as obtained by MC simulations. The centres of nearest neighbours are connected by lines. Samples a) 1, b) 2 and c) 5 are shown.

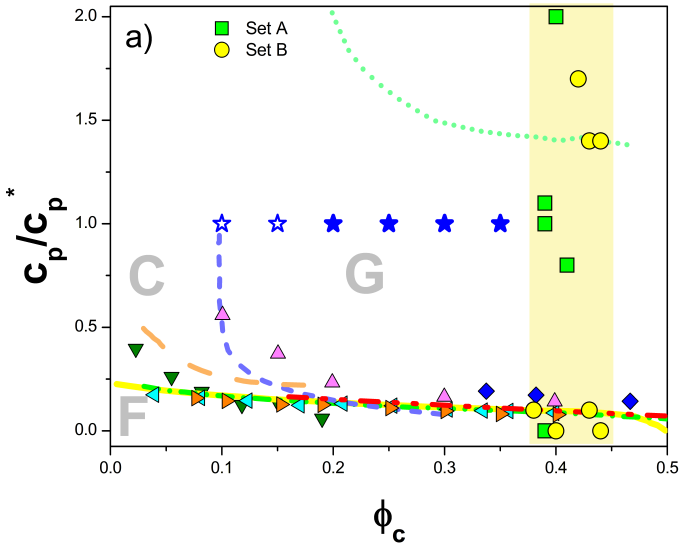

Fig. 8 State diagram of a colloid-polymer mixture with a size ratio $\xi \sim 0.1$ in the polymer concentration, c_p/c_p^*, *vs.* colloid volume fraction, ϕ_c, plane. Region covered by our samples (■: set 1, ●: set 2) is highlighted by a yellow background (Table 1), 'F' indicates fluid states and 'G' gel states, ☆, ★: additional simulation results for $c_p/c_p^* = 1.0$ and different ϕ_c where open (full) symbols indicate fluid (gel) states. Binodal line obtained using the Generalised Free Volume Theory[42,43] for $\xi = 0.076$ (- · - · -). For comparison, data sets from literature are included: equilibrium fluid-solid coexistence for $\xi = 0.08$[16] (——), experimentally determined gelation points in purely attractive systems with $\xi = 0.061$[38] (◂), $\xi = 0.090$[38] (▸), $\xi = 0.06$[60] (▲), $\xi = 0.059$[20] (– – –) and in systems with competing interactions with $\xi = 0.021$[18] (▼), $\xi = 0.13$[25] (- - -), $\xi = 0.19$[19] (·····), experimentally observed attractive glasses with $\xi = 0.09$[61] (◆), Mode-Coupling predictions for the gelation boundaries for $\xi = 0.08$[21] (- · - ·).

ing polymer concentration a coexistence between fluid and crystal is observed (solid line represents the fluid/solid coexistence boundary for $\xi = 0.08$[16]). Gas-liquid coexistence occurs within the fluid-solid coexistence region[16]: We report in Fig. 8 the binodal line (double-dotted–dashed line), calculated using the Generalised Free Volume Theory[42,43] for the size ratio of our samples, $\xi = 0.076$. We additionally report the boundaries to non-equilibrium gel states determined by different experiments and theories. For small volume fractions ($\phi_c < 0.2$), we show the gelation boundary obtained by Lu et al.[20] (large-dashed line, $\xi = 0.059$): in this work it is proposed that frustrated gas-liquid phase separation leads to the gel transition, and hence the gel states are expected inside the spinodal line. Furthermore, we show predictions of mode-coupling theory from Bergenholtz and coworkers for the gel boundary[21] extending over the whole ϕ_c range (dashed-dotted line, $\xi = 0.08$). The theory results are complemented by experimentally determined gel boundaries obtained by Shah and coworkers for $\xi = 0.061$ and 0.090[38], and Poon and coworkers for $\xi \sim 0.06$[60]. Finally, we also plot the boundary between fluid and attractive glass determined by Pham and coworkers for $\xi = 0.09$[61]. As can be observed, the gel boundaries predicted by theory and observed in experiments are all lying close to or above the binodal line. This finding apparently supports the scenario in which arrested spinodal decomposition leads to gel formation[20]. However, recent studies indicate that this scenario is correct at low particle concentrations, while the role of rigidity percolation might be important at higher ϕ_c[59,62]. Moreover, we can observe that generally the transition from equilibrium fluid states to non-equilibrium solid states, either gel or glass, occurs at low polymer concentrations in systems where the interactions are purely attractive.

In comparison, systems with competing interactions exhibit a richer and more complex behaviour that also depends on the range and strength of the repulsive interaction. If a repulsive barrier is present, the binodal tends to disappear and a cluster fluid phase is found instead[3,25,63]. In systems of highly charged colloids, at low concentrations $\phi_c < 0.17$ also other states are present, such as Wigner glasses and glassy cluster states[19], while at moderate concentrations $0.15 < \phi_c < 0.30$ gel states are still being observed. In Fig. 8 we report the experimentally determined depletion boundaries for colloids

with competing interactions from Campbell and coworkers, for $\xi = 0.13$, $\kappa\sigma \approx 1.55$ and $Z^2 = 30$[25], from Klix and coworkers for $\xi = 0.19$, $\kappa\sigma \approx 1$ and $Z^2 = 15$[19], and from Sedgwick and coworkers for $\xi = 0.021$[18] (values for the repulsive interaction could not be estimated in this case). In these and other studies[38,60] a cluster phase is observed in the same interval $0.03 \leq c_\mathrm{p}/c_\mathrm{p}^* \leq 2.0$, but at lower ϕ_c. We observe that the effect of the additional repulsive interaction is that of shifting the gel boundary to higher ϕ_c and larger c_p values when κ decreases and hence the range of the electrostatic interactions increases.

The values of $\kappa\sigma$, ξ and Z^2 of our potential are even larger than those of the work of Campbell and coworkers[25]. We can therefore expect that the gel boundary lies at relatively low polymer concentrations and approaches that of purely attractive systems. This seems to be confirmed by the experimental data (Fig. 8), where, in the absence of polymer and at small polymer concentration, we observe fluid states close to the gelation boundaries of the purely attractive systems and the data of[25], if extrapolated to larger ϕ_c. At the same time, gel states are found well below the gelation boundary of[19].

We have also performed simulations at constant $c_\mathrm{p}/c_\mathrm{p}^* = 1.0$ and different volume fractions, with the potential parameters describing sample 3, indicate that the gelation boundary is slightly shifted compared to the data in[25] (Fig. 8), and especially that gel states are not observed at small ϕ_c, in contrast with the purely attractive case. Snapshots of the simulations are shown in Fig. 9, where only particles participating in clusters with at least 5 particles are shown. At $\phi_\mathrm{c} < 0.15$ small clusters are dispersed throughout the volume (these states are indicated as empty stars in Fig. 8). At $\phi_\mathrm{c} = 0.20$ larger clusters are formed, probably percolated, which indicates that the system is close to the gelation boundary, and at higher concentrations, $\phi_\mathrm{c} \geq 0.25$, large clusters dominate, consistent with the state diagram (these states are indicated as filled stars in Fig. 8).

We can therefore conclude that, even if our effective potential is strongly screened, the state diagram of our system does not seem to be fully compatible with that of a purely attractive system, but rather indicates the effects of competing attractive and repulsive interactions.

3.5 Second virial coefficient

The effective colloid–colloid interaction potential is characterised by a short-range attraction and a longer-ranged repulsion. This interplay determines the arrangement of the particles. However, due to the large volume fractions $0.38 \leq \phi_\mathrm{c} \leq 0.44$ (Table 1) crowding also plays a significant role. To quantify the different contributions to the interactions, for all samples with $c_\mathrm{p}/c_\mathrm{p}^* > 0.1$ (Table 2) we have calculated the

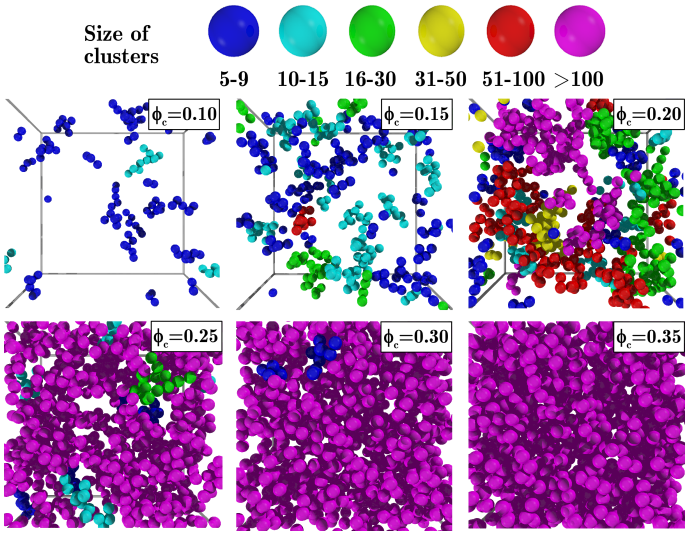

Fig. 9 Snapshots of systems at $c_\mathrm{p}/c_\mathrm{p}^* = 1$ for different colloidal volume fractions ϕ_c obtained from simulations with the size of the clusters in which the particle participates indicated by the colour of the particle. These systems are indicated by open (non-percolated states) and filled (percolated states) blue stars in Fig. 8.

reduced second virial coefficient $B_2^* \equiv B_2/B_2^{\mathrm{HS}}$[48,59], where B_2 is the second virial coefficient and B_2^{HS} the one of hard-spheres. For set A, $B_2^* > 0$, which indicates a strong effect of the repulsive component, while for set B, $B_2^* < 0$, which means that the attractive contribution dominates. Thus, the gel structure in our samples is determined by crowding combined with either dominantly repulsive (set A) or dominantly attractive (set B) interactions. A theoretical analysis of the binodal for $\xi = 0.076$ nevertheless suggests that all gel samples studied here are well inside the phase separation region (Fig. 8). However, none of the samples, particularly the ones in set A (where repulsion dominates), reach the value $B_2^* = -1.5$[64]. This value has been associated with the proximity of phase separation in systems with attractive pair potentials. This requires that the attractions are short-ranged, $\xi < 0.15$, and hence many-body effects are excluded[?], which is the case in our samples. Thus, a more complex mechanism seems to be responsible for the gel transition at intermediate colloid volume fractions and especially in the presence of electrostatic repulsion.

4 Discussion and Conclusions

The results presented in the previous section can be summarised to obtain a general picture of the system under investigation: In the absence of polymers ($c_\mathrm{p} = 0.0$), the structure of the samples, namely homogeneously distributed particles in a colloidal fluid, can be described by a repulsive Yukawa poten-

tial, which is due to the residual charges (Fig.2a,b) . The addition of a small amount of polymers ($c_\mathrm{p}/c_\mathrm{p}^* = 0.1$) induces the formation of a few small clusters due to depletion attractions. However, the electrostatic repulsion dominates and the systems remain fluid and essentially homogeneous (Fig.2c). Instead, with increasing amount of polymer ($0.8 \leq c_\mathrm{p}/c_\mathrm{p}^* \leq 2.0$), the attractions become more pronounced, as shown by the effective potentials obtained (Table 2) and clusters are formed which merge into a network gel structure. The radial distribution functions indicate for all gel samples a strong and short-ranged correlation between particles. However, even if the interaction potential is different, the $g(r)$ of the gels is relatively similar within each set of samples (Fig.3, for sets A and B), but a flatter region around the minimum is observed for samples of set B. Similarly, the angular distribution functions also indicate comparable internal cluster structures within one set, with particles forming triangular and tetrahedral structures as indicated by peaks at 60° and 120°. The nearest-neighbour distributions are also similar within one set, but set B presents higher average numbers of neighbours. These results suggest that the structure of the gels is not particularly sensitive to variations in the strength of attractions at fixed screening (i.e., within a set), where the attraction strength ranges from $0.8\,k_\mathrm{B}T$ to $1.4\,k_\mathrm{B}T$, i.e. around the thermal energy. In contrast, the structural differences between the two sets A and B suggest a stronger influence of the electrostatic interactions, which also cover a larger range (Fig. 4b). These observations were complemented by calculations of the second virial coefficient for samples of the two sets (Table 2): we observed that, in addition to crowding, for set A gel formation is dominated by repulsion and for set B by attraction. These results indicate that the variation of the electrostatic contribution, which also induces variations in the effective attraction at short distances, is crucially affecting the gel structure.

By comparison with previous work on state diagrams of colloid-polymer systems, and our own calculations of the binodal line, we could additionally confirm that even if the repulsive electrostatic interactions are strongly screened, the structures that we observe are compatible with the state diagrams expected and observed for colloid-polymer mixtures with competing interactions.

In conclusion, we were able to describe the non-equilibrium structures of intermediate volume fraction gels observed in experiments by using a simple effective pair interaction potential although non-equilibrium effects are not explicitly considered. The effective interaction potential thus not only depends on the sample composition, but also the preparation history. Therefore, if the preparation path and hence maybe the gel structure are changed, also the effective interaction potential will change. Nevertheless, the effective interaction potentials and their parameters, which were determined by comparing the radial distribution function $g(r)$ obtained by experiments and simulations, respectively, were successfully used to predict other structural features, such as the angular distribution function $P(\theta)$ and the nearest-neighbour distribution function $P(n_\mathrm{b})$, as well as the state diagram. The effective interaction potential contains a short-range attraction modelled through a square-well and longer-ranged electrostatic repulsion modelled though a Yukawa form. Through the parameters of the potential we can assess the relative contribution of the attractive and the repulsive component on the gel structure. We found that the degree of screening of the electrostatics has an important influence on the structural organisation since it significantly affects the balance between repulsive and attractive interactions. Due to that, we observed different gel structures which are dominated by either repulsion or attraction.

Acknowledgments

We thank Andrew Schofield (The University of Edinburgh) for the PMMA particles. This work was supported by the International Helmholtz Research School of Biophysics and Soft Matter (IHRS BioSoft), by the Deutsche Forschungsgemeinschaft (DFG) and grant INST 208/617-1FUGG funding the confocal microscope, by CONACyT (grant No. 237425) and by the Universidad de Guanajuato (Convocatoria Institucional de Investigación Científica 2016-2017). R. C.-P. acknowledges the financial support provided by the Marcos Moshinsky fellowship 2013-2014 and the Alexander von Humboldt Foundation supporting his stay at the University of Düsseldorf during the summer 2016.

References

1 Y. Liu, L. Porcar, J. Chen, W.-R. Chen, P. Falus, A. Faraone, E. Fratini, K. Hong and P. Baglioni, *J. Phys. Chem. B*, 2011, **115**, 7238–7247.
2 Y. Liu, *Chem. Eng. Process. Tech.*, 2013, **1**, 2–5.
3 A. Stradner, H. Sedgwick, F. Cardinaux, W. C. K. Poon, S. U. Egelhaaf and P. Schurtenberger, *Nature*, 2004, **432**, 492–495.
4 S. Yadav, T. M. Laue, D. S. Kalonia, S. N. Singh and S. J. Shire, *Mol. Pharm.*, 2012, **9**, 791–802.
5 K. P. Johnston, J. A. Maynard, T. M. Truskett, A. U. Borwankar, M. A. Miller, B. K. Wilson, A. K. Dinin, T. A. Khan and K. J. Kaczorowski, *ACS Nano*, 2012, **6**, 1357–1369.
6 E. Yearley, I. Zarraga, S. Shire, T. Scherer, Y. Gokarn, N. Wagner and Y. Liu, *Biophys. J*, 2013, **105**, 720 – 731.
7 E. Yearley, P. Godfrin, T. Perevozchikova, H. Zhang, P. Falus, L. Porcar, M. Nagao, J. Curtis, P. Gawande, R. Taing, I. Zarraga, N. Wagner and Y. Liu, *Biophys. J*, 2014, **106**, 1763 – 1770.
8 E. Zaccarelli, *J. Phys. Condens. Matter*, 2007, **19**, 323101.
9 T. Sentjabrskaja, E. Zaccarelli, C. De Michele, F. Sciortino, P. Tartaglia, T. Voigtmann, S. U. Egelhaaf and M. Laurati, *Nat. Commun.*, 2016, **7**, 11133.
10 E. Mani, E. Sanz, P. G. Bolhuis and W. K. Kegel, *The J. Phys. Chem. B*, 2010, **114**, 7780–7786.
11 W. C. K. Poon, *J. Phys. Condens. Matter*, 2002, **14**, R859–R880.
12 A. Yethiraj and A. van Blaaderen, *Nature*, 2003, **421**, 513–517.
13 S. Asakura and F. Oosawa, *J. Polym. Sci.*, 1958, **33**, 183.

14 F. Oosawa and S. Asakura, *J Chem. Phys.*, 1954, **22**, 1255.

15 H. N. W. Lekkerkerker, W. Poon, P. Pusey, A. Stroobants and P. B. Warren, *Europhys. Lett.*, 1992, **20**, 559–564.

16 S. M. Ilett, A. Orrock, W. C. K. Poon and P. N. Pusey, *Phys. Rev. E*, 1995, **51**, 1344–1352.

17 S. Ramakrishnan, M. Fuchs, K. S. Schweizer and C. F. Zukoski, *J. Chem. Phys.*, 2002, **116**, 2201.

18 H. Sedgwick, S. U. Egelhaaf and W. C. K. Poon, *J. Phys. Condens. Matter*, 2004, **16**, S4913.

19 C. L. Klix, C. P. Royall and H. Tanaka, *Phys. Rev. Lett.*, 2010, **104**, 165702.

20 P. J. Lu, E. Zaccarelli, F. Ciulla, A. B. Schofield, F. Sciortino and D. A. P. C. B. Weitz, *Nature*, 2008, **453**, 499–503.

21 J. Bergenholtz, W. C. K. Poon and M. Fuchs, *Langmuir*, 2003, **19**, 4493–4503.

22 S. Shah, Y. Chen, S. Ramakrishnan, K. Schweizer and C. Zukoskoi, *J. Phys. Condens. Matter*, 2003, **15**, 4751–4778.

23 N. E. Valadez-Pérez, Y. Liu, A. P. R. Eberle, N. J. Wagner and R. Castañeda-Priego, *Phys. Rev. E*, 2013, **88**, 060302(R).

24 C. Patrick Royall, S. R. Williams, T. Ohtsuka and H. Tanaka, *Nat. Mat.*, 2008, **7**, 556–561.

25 A. I. Campbell, V. J. Anderson, J. S. van Duijneveldt and P. Bartlett, *Phys. Rev. Lett.*, 2005, **94**, 208301.

26 F. Sciortino, P. Tartaglia and E. Zaccarelli, *J. Phys. Chem. B*, 2005, **109**, 21942–21953.

27 E. Mani, W. Lechner, W. K. Kegel and P. G. Bolhuis, *Soft Matter*, 2014, **10**, 4479–86.

28 M. Kohl, R. F. Capellmann, M. Laurati, S. U. Egelhaaf and M. Schmiedeberg, *Nat. Commun.*, 2016, **7**, 11817.

29 P. A. Smith, G. Petekidis, S. U. Egelhaaf and W. C. K. Poon, *Phys. Rev. E*, 2007, **76**, 041402.

30 J. C. F. Toledano, F. Sciortino and E. Zaccarelli, *Soft Matter*, 2009, **5**, 2390–2398.

31 I. Zhang, C. P. Royall, M. a. Faers and P. Bartlett, *Soft Matter*, 2013, **9**, 2076.

32 P. Varadan and M. J. Solomon, *Langmuir*, 2003, **19**, 509–512.

33 G. Foffi, C. De Michele, F. Sciortino and P. Tartaglia, *J. Chem. Phys.*, 2005, **122**, 224903.

34 M. Laurati, G. Petekidis, N. Noumakis, F. Cardinaux, A. Schofield, J. Brader, M. Fuchs and S. Egelhaaf, *J. Chem. Phys.*, 2009, **130**, 134907.

35 C. P. Royall, D. G. A. L. Aarts and H. Tanaka, *J. Phys. Condens. Matter*, 2005, **17**, S3401.

36 C. P. Royall, M. E. Leunissen, A.-P. Hynninen, M. Dijkstra and A. van Blaaderen, *J. Chem. Phys.*, 2006, **124**, 244706.

37 C. L. Klix, K.-i. Murata, H. Tanaka, S. R. Williams, A. Malins and C. P. Royall, *Sci. Rep.*, 2013, **3**, 2072.

38 S. A. Shah, Y.-L. Chen, K. S. Schweizer and C. F. Zukoski, *J. Chem. Phys.*, 2003, **119**, 8747–8760.

39 C. P. Royall, A. A. Louis and H. Tanaka, *J. Chem. Phys.*, 2007, **127**, 044507.

40 M. G. Noro and D. Frenkel, *J. Chem. Phys.*, 2000, **113**, 2941–2944.

41 G. C. Berry, *J. Chem. Phys.*, 1966, **44**, 4550.

42 G. J. Fleer and R. Tuinier, *Phys. Rev. E*, 2007, **76**, 041802.

43 H. N. W. Lekkerkerker, W. C. K. Poon, P. N. Pusey, A. Stroobants and P. B. Warren, *Europhys. Lett.*, 1992, **20**, 559.

44 C. P. Royall, W. C. K. Poon and E. R. Weeks, *Soft Matter*, 2013, **9**, 17–27.

45 J. C. Crocker and D. G. Grier, *J. Colloid Interface Sci.*, 1996, **179**, 298 – 310.

46 M. Jenkins and S. Egelhaaf, *Adv. Colloid Interface Sci.New J. Phys.*, 2008, **136**, 65–92.

47 E. Schöll-Paschinger, A. L. Benavides and R. Castañeda-Priego, *J. Chem. Phys.*, 2005, **123**, 234513.

48 N. E. Valadez-Pérez, A. L. Benavides, E. Schöll-Paschinger and R. Castañeda-Priego, *J. Chem. Phys.*, 2012, **137**, 084905.

49 F. Platten, N. E. Valadez-Pérez, R. Castañeda-Priego and S. U. Egelhaaf, *J. Chem. Phys.*, 2015, **142**, 174905.

50 S. Bucciarelli, N. Mahmoudi, L. Casal-Dujat, M. Jehannin, C. Jud and A. Stradner, *J. Phys. Chem. Lett.*, 2016, **7**, 1610–1615.

51 J. Dobnikar, R. Castañeda-Priego, H. H. von Grünberg and E. Trizac, *New J. Phys.*, 2006, **8**, 277.

52 L. F. Rojas-Ochoa, R. Castañeda-Priego, V. Lobaskin, A. Stradner, F. Scheffold and P. Schurtenberger, *Phys. Rev. Lett.*, 2008, **100**, 178304.

53 E. Trizac, L. Belloni, J. Dobnikar, H. H. von Grünberg and R. Castañeda Priego, *Phys. Rev. E*, 2007, **75**, 011401.

54 B. D'Aguanno and R. Klein, *J. Chem. Soc., Faraday Trans.*, 1991, **87**, 379–390.

55 G. V. Schulz, *Z. Physik. Chem.*, 1939, **B43**, 25.

56 M. P. Allen and D. J. Tildesley, *Computer Simulations of Liquids*, Oxford Science Publications, 1989.

57 D. Frenkel and B. Smith, *Understanding Molecular Simulation, Second Edition: From Algorithms to Applications (Computational Science)*, Academic Press, 2001.

58 E. López-Sánchez, C. D. Estrada-Alvarez, G. Pérez-Angel, J. M. Méndez-Alcaraz, P. González-Mozuelos and R. Castañeda-Priego, *J. Chem. Phys.*, 2013, **139**, 104908.

59 N. E. Valadez-Perez, R. Castañeda-Priego and Y. Liu, *RSC Adv.*, 2013, **3**, 25110–25119.

60 W. C. K. Poon, L. Starrs, S. P. Meeker, A. Moussaid, R. M. L. Evans, P. N. Pusey and M. M. Robins, *Faraday Discuss.*, 1999, **112**, 143–154.

61 K. N. Pham, S. U. Egelhaaf, P. N. Pusey and W. C. K. Poon, *Phys. Rev. E*, 2004, **69**, 011503.

62 A. P. R. Eberle, N. J. Wagner and R. Castañeda Priego, *Phys. Rev. Lett.*, 2011, **106**, 105704.

63 P. D. Godfrin, N. E. Valadez-Perez, R. Castañeda-Priego, N. J. Wagner and Y. Liu, *Soft Matter*, 2014, **10**, 5061–5071.

64 G. A. Vliegenthart and H. N. W. Lekkerkerker, *J. Chem. Phys.*, 2000, **112**, 5364–5369.